α-MnO$_2$/FeCo-LDH on Nickel Foam as an Efficient Electrocatalyst for Water Oxidation

Saeedeh Shahparast and Karim Asadpour-Zeynali*

Cite This: *ACS Omega* 2023, 8, 1702−1709

Read Online

ACCESS | Metrics & More | Article Recommendations | Supporting Information

ABSTRACT: The ever-expanding human societies on the one hand and the diminishing fossil fuel resources on the other have driven man to find a suitable, cheap, clean, and accessible source of energy. Water splitting is a good solution to this crisis. Because of the slow kinetics of water oxidation reaction, it is important to select efficient and durable electrocatalysts to improve the reaction kinetics. In this research, α-MnO$_2$/FeCo-LDH catalysts on nickel foam were developed for water oxidation, which exhibited good catalytic performance and stability in a 0.1 M KOH solution. The electrocatalysts were synthesized by hydrothermal methods and characterized by XRD, FTIR, Raman, SEM, TEM, EDS, and MAP techniques. The proposed modified electrode has large exchange current, low overpotential, and small Tafel slope. Here, only an overpotential of 210 mV is required to achieve a current density of 5 mA cm^2 with a Tafel slope of 70.4 mV dec^{-1} in an alkaline solution.
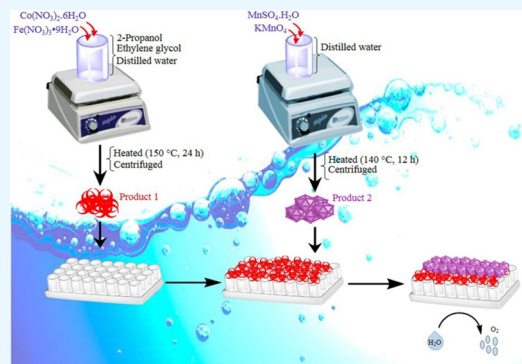
1. INTRODUCTION

Energy production is one of the greatest challenges facing human society. Given the depletion of fossil fuel resources, the growing world population, and the increasing demand for energy, it is very important to substitute clean, cheap, and environmentally friendly renewable energy sources.[1] Hydrogen fuel is a practical and simple solution to this problem. Hydrogen is a clean and inexpensive fuel that does not have the problems of fossil fuels, such as pollution, limited resources, and toxicity of combustion products, and therefore has been considered in recent years.[2] A good way to produce hydrogen is electrochemical water splitting. The water splitting is based on the hydrogen reaction and the oxygen evolution reaction.[3] The oxygen evolution reaction has slow, complex, and multistep kinetics, so the use of effective and inexpensive electrocatalysts that can reduce the overvoltage required for water oxidation and improve reaction kinetics is essential.[4] Various catalysts can be used for this purpose. Catalysts based on transition-metal oxides and LDHs offer promising prospects.[5] Precious metal oxides such as Ru and Ir have good stability and performance in water oxidation, but because their sources are limited and precious, their use is limited. For this reason, metal oxides based on first-row transition metals are preferred. In recent years, studies have been conducted on the use of transition-metal oxides such as Fe$_2$O$_3$, MnO$_2$, ZnO, and Co$_3$O$_4$ in water oxidation. Layered double hydroxides (LDHs) are good electrocatalysts with a high ability to oxidize water. LDHs are a group of bilayer materials consisting of positively charged metal hydroxides with anions trapped between the layers. The general structure of LDHs is M^{II}(OH)$_2$, where M^{II} can be replaced by M^{III} ions and the extra positive charge is balanced by the anions. M^{2+} can contain elements such as Mg^{2+}, Ca^{2+}, Cu^{2+}, Mn^{2+}, Ni^{2+} and M^{3+} including Al^{3+}, Cr^{3+}, Fe^{3+}, Mn^{3+}, and Co^{3+}.[6]

Various methods have been proposed for the synthesis of LDHs, including the hydrothermal technique of coprecipitation, electrical deposition, and sol−gel.[7] LDHs can also be obtained by anion exchange of a recrystallized LDH clay. Recently, LDHs based on transition metals have been introduced because of their attractive properties such as special structure, abundance in nature, environmental friendliness, high corrosion resistance, ductility, large surface area, low cost, electrical conductivity, good stability, easy fabrication, and adaptability to the respective compounds.[8] Because of the above properties, they have found various and wide applications, which can be mentioned as follows: in fuel cells,[9] as catalysts,[10] in drug delivery,[11] in biotechnology and biosensors,[12] in adsorbents,[13] and as flame retardants.[14] LDHs reduce the overvoltage required for hydrogen production, which make them good electrocatalysts for water oxidation.[15]

Nickel is more conductive in alkaline environments, and nickel sites increase hydrolysis, whereas cobalt sites increase
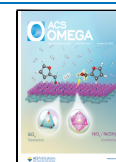
hydrogen release.[16] Therefore, LDH containing these elements has good electrochemical advantages. Other reasons for using nickel as a substrate include its high electrical conductivity, three-dimensional network structure, low toxicity, and low cost.

Various electrochemical studies performed with manganese-containing compounds and manganese oxides have shown that manganese oxide acts as an electrocatalyst with good performance. For example, Zhang and co-workers used MnO_x for the oxidation of water.[17] In another study, Teng and co-workers demonstrated that Fe−Mn−O hybrid nanosheets can be successfully used for water oxidation.[18] Numerous and varied examples have also been reported for manganese and its compounds.[19] LDHs containing the elements nickel, iron, and cobalt with double capacity are good catalysts for water oxidation in alkaline environments.

In this work, α-MnO_2 nanoparticles were intercalated as a second layer into the first layer of FeCo-LDH immobilized on a nickel foam substrate. We present a convenient and simple method for the preparation of α-MnO_2-Fe-Co LDH by hydrothermal methods. The morphology and purity of the synthesized products were studied by X-ray diffraction (XRD), field emission scanning electron microscopy (FESEM), transmission electron microscope (TEM), Brunauer−Emmett−Teller (BET), energy-dispersive X-ray spectroscopy (EDS), element mapping (MAP), Fourier transform IR (FTIR), and Raman. The electrocatalytic activity of the product was investigated by linear sweep voltammograms (LSVs) and Tafel analysis. In addition, the long-term stability of the synthesized materials in an alkaline medium was investigated at OER by repeated amperometry and continuous LSV tests. The innovation of this manuscript is the synergistic effect of the two desired compounds in the final catalyst (α-MnO_2/FeCo-LDH/NF) compared to the individual components, showing the improvement of electrocatalytic performance in OER.

2. EXPERIMENTAL SECTION

2.1. Apparatus and Reagents. An EG&G Model 273 Potentiostat/Galvanostat was used for the electrochemical measurements. The electrochemical system used consisted of three electrodes: nickel foam, rectified with the catalyst, as the working electrode; Ag/AgCl as the reference electrode; and stainless steel sheet as the counter electrode (all electrodes were purchased from Azar Electrode Company, Urmia, Iran). Iron(III) nitrate nonahydrate ($Fe(NO_3)_3 \cdot 9H_2O$), cobalt(II) nitrate hexahydrate ($Co(NO_3)_2 \cdot 6H_2O$), manganese(II) sulfate monohydrate ($MnSO_4 \cdot H_2O$), potassium permanganate ($KMnO_4$), potassium hydroxide (KOH, ≥97.0%), 2-propanol ($CH_3CHOHCH_3$), and ethylene glycol ($(CH_2OH)_2$) were purchased from Merck and used for the experiments. Distilled water was used to prepare the chemical solutions. All these materials were purchased from Merck (Germany).

2.2. Preparation of Nickel Foam (NF) Electrodes. Several pieces of nickel foam (0.5×1 cm^2) were washed in an ultrasonic bath with a 3 M HCl solution for 10 min to remove surface contaminants. Then, the nickel foams were placed in an ultrasonic bath containing acetone, ethanol, and distilled water, successively, for 10 min to remove surface impurities.

2.3. Synthesis of α-MnO_2-Fe-Co LDH/NF. First, Fe-$(NO_3)_3 \cdot 9H_2O$ (0.24 mmol) and $Co(NO_3)_2 \cdot 6H_2O$ (0.72 mmol) were dissolved in a mixture of 2-propanol solvents (15 mL), ethylene glycol (5 mL), and distilled water (15 mL);

stirred for 30 min; and brought to pH = 9.5 with NaOH (1 M). The resulting solution was then degassed with nitrogen gas and placed in a 100 mL autoclave at 150 ° C for 24 h. After the desired time elapsed and the temperature of the autoclave reached room temperature, the precipitate was removed from the solvent by centrifugation and washed several times with distilled water to remove residual ions. The synthesized product was placed in a desiccator for 3 days. To prepare FeCo-LDH on NF, 5 mg of synthesized FeCo-LDH was ultrasonically dispersed in 1 mL of ethanol for half an hour. Ten microliters of the suspension was dropped onto the clean NF surface and dried at room temperature for 24 h. After drying the droplet, FeCo-LDH/NF was obtained. The synthesis of α-MnO_2 was carried out according to the literature.[20]

To synthesize α-MnO_2, $MnSO_4 \cdot H_2O$ (0.2 g) and $KMnO_4$ (0.5 g) were dissolved in 35 mL of distilled water and stirred for 20 min to obtain a homogeneous solution. The solution was placed in a 100 mL autoclave at 140 ° C for 12 h. After the temperature of the autoclave reached room temperature, the resulting product was centrifuged and washed several times with distilled water, and after drying, the α-MnO_2 product was obtained. To prepare α-MnO_2/FeCo-LDH/NF, 5 mg of α-MnO_2 powder was ultrasonically dispersed in 1 mL of ethanol for half an hour. Ten microliters of the suspension was dropped onto the FeCo-LDH/NF and then dried at room temperature for 24 h to obtain the final electrode (α-MnO_2/FeCo-LDH/NF).

3. RESULTS AND DISCUSSION

3.1. Product Characterization. The synthesized products were identified by different techniques, and their electrocatalytic performance was studied. XRD analysis was performed to analyze the structure ($2\theta = 10-80°$). The X-ray diffraction pattern of FeCo-LDH is shown in Figure 1a.

There are two main peaks at $2\theta = 11.44$ and 23.3°, which are a good confirmation of the LDH structure. The peaks of the FeCo-LDH XRD pattern show the scattering of nanoparticles at 33.9, 35.46, 38.42, 44.42, 47.11, 59.36, and 60.44° and can be indexed to (012), (009), (015), (107), (019), (110), and (113) (JCPDS Card No. 50-0235).[21] Figure 1b shows the XRD patterns of α-MnO_2 nanoparticles. As shown, the peaks at 2θ of 12.34, 17.94, 27.06, 36.68, 41.82, 49.27, 57.62, 60.61, 65.20, 68.78, and 72.66° correspond to (110), (200), (310), (211), (301), (411), (600), (521), (002), (541), and (332), respectively, demonstrating the high purity of the synthesized nanoparticles (ICCD-JCPDS Card No. 44-0141).[20]

The FTIR spectrum of the synthesized products is shown in Figure 1c,d. The FeCo-LDH shows a broad absorption at 3428 and 1633 cm^{-1}, which is related to the vibration of the OH group.[22] The vibration of the NO_3^- group is observed at 1355 cm^{-1}.[23] The band at 661 cm^{-1} is related to Co−O vibrations,[24] and other bands including 745 and 1001 cm^{-1} are related to Fe−O vibrations (Figure 1c).[25] Figure 1d shows the FTIR spectrum of α-MnO_2 nanoparticles. Here, we also see the vibrations of the OH group (3377 and 1623 cm^{-1}). The peak at 1393 cm^{-1} is related to the O_2 bending, and the sharp peak at 523 cm^{-1} shows the vibrational frequency of the Mn−O band.[26] Raman spectra of the synthesized nanoparticles were acquired. The FeCo-LDH has peaks at 553 and 670 cm^{-1}, which represent the Fe−O and Co−O groups, respectively (Figure 1e).[27] The peak at 582 cm^{-1} indicates the Mn−O
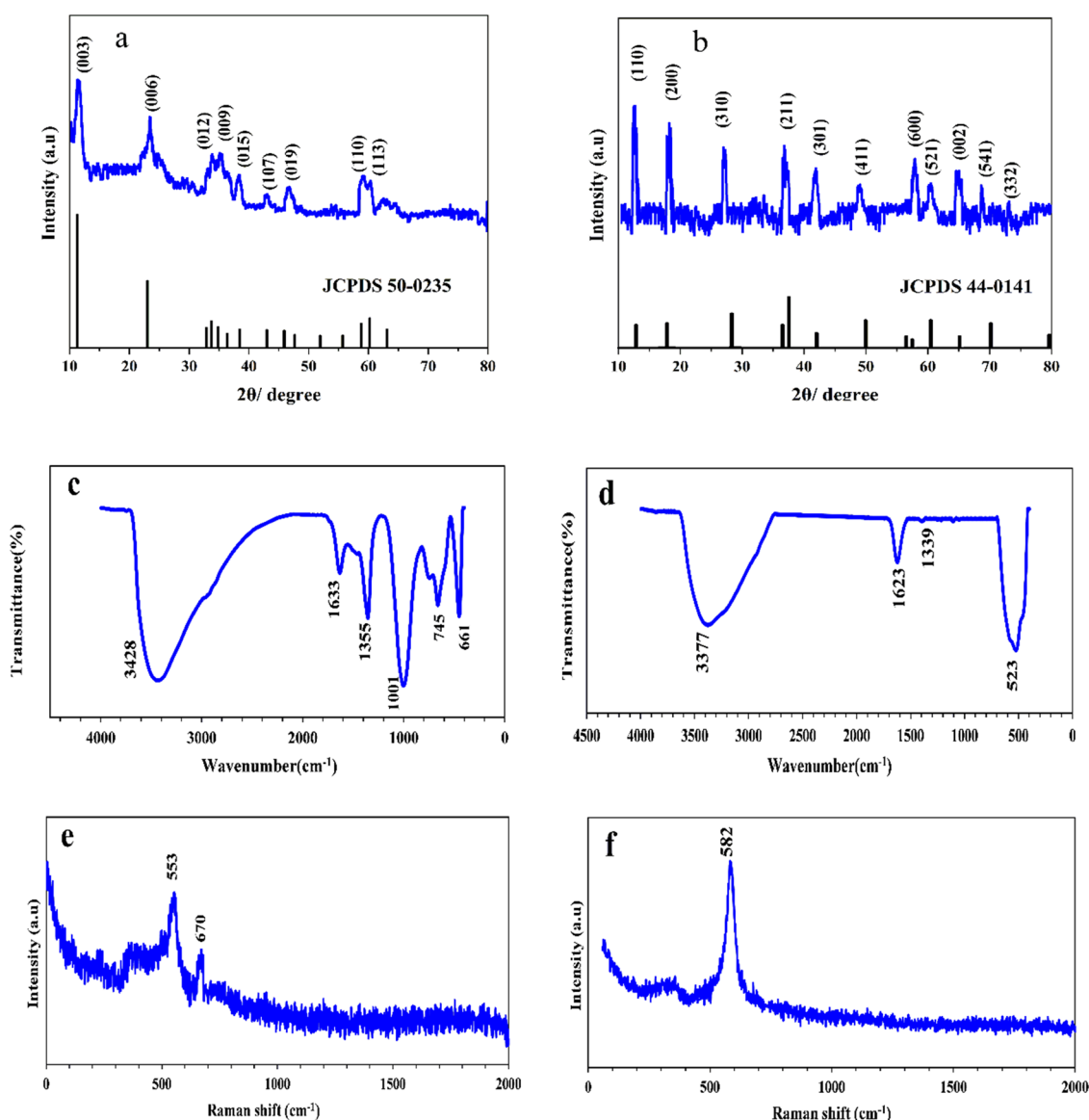
Figure 1. XRD patterns of (a) FeCo-LDH and (b) α-MnO$_2$ nanoparticles, FTIR spectra of (c) FeCo LDH and (d) α-MnO$_2$, and Raman spectra of (e) FeCo LDH and (f) α-MnO$_2$.

vibration, which is a good indication of the formation of α-MnO$_2$ products (Figure 1f).[28]

FESEM analysis was performed to study the structure and morphology of the products. Figure 2a,b shows the SEM images of FeCo-LDH/NF. As can be seen, FeCo-LDH exhibits a sheet-like structure with a length of ~250 nm and a thickness of ~27 nm. Figure 2c,d shows the structure of α-MnO$_2$/NF nanosheets with a length of several micrometers and a thickness of 21 nanometers. Figure 1e,f shows the SEM images of α-MnO$_2$/FeCo-LDH/NF. In addition, the morphology and structure of the synthesized nanoparticles were evaluated by TEM analysis. Figure 2g–j shows the TEM images of FeCo-LDH and α-MnO$_2$ powders. The results of TEM analysis also confirm the sheet-like structure of the synthesized nanoparticles.

For further investigation, the chemical structure of the synthesized catalysts was evaluated by EDS. Figure S1a–c shows the results of this analysis, which demonstrate the presence of Fe and Co elements in FeCo LDH/NF and Mn and O in α-MnO$_2$/NF, as well as all of these elements in α-

MnO$_2$/FeCo-LDH/NF. The data obtained from MAP analysis indicate the presence of Fe and Co elements in FeCo-LDH and Mn and O in α-MnO$_2$ nanoparticles. These elements are also present in α-MnO$_2$/FeCo-LDH. The presence and homogeneous distribution of the elements indicate the successful synthesis of the products (Figure S1d–q).

To investigate the porosity and the particular surface area of the nanoparticles, BET analysis was performed; the results are shown in Figure 3a,b. Adsorption and desorption were performed with N$_2$ gas at 77 K. According to the results of the analysis, the BET specific surface areas of FeCo-LDH and α-MnO$_2$ were 95.139 and 95.853 m^2 g^{-1}, respectively. The high specific surface area increases the active sites of the reaction and decreases the charge transfer resistance, which improves the electrocatalytic performance of the electrode.

3.2. Electrochemical Measurements. Electrochemical measurements were performed in a three-electrode system with a solution of 0.1 M KOH (pH = 13). The electrodes used in this system were Ag/AgCl as the reference electrode, nickel foam rectified with LDH as the working electrode, and
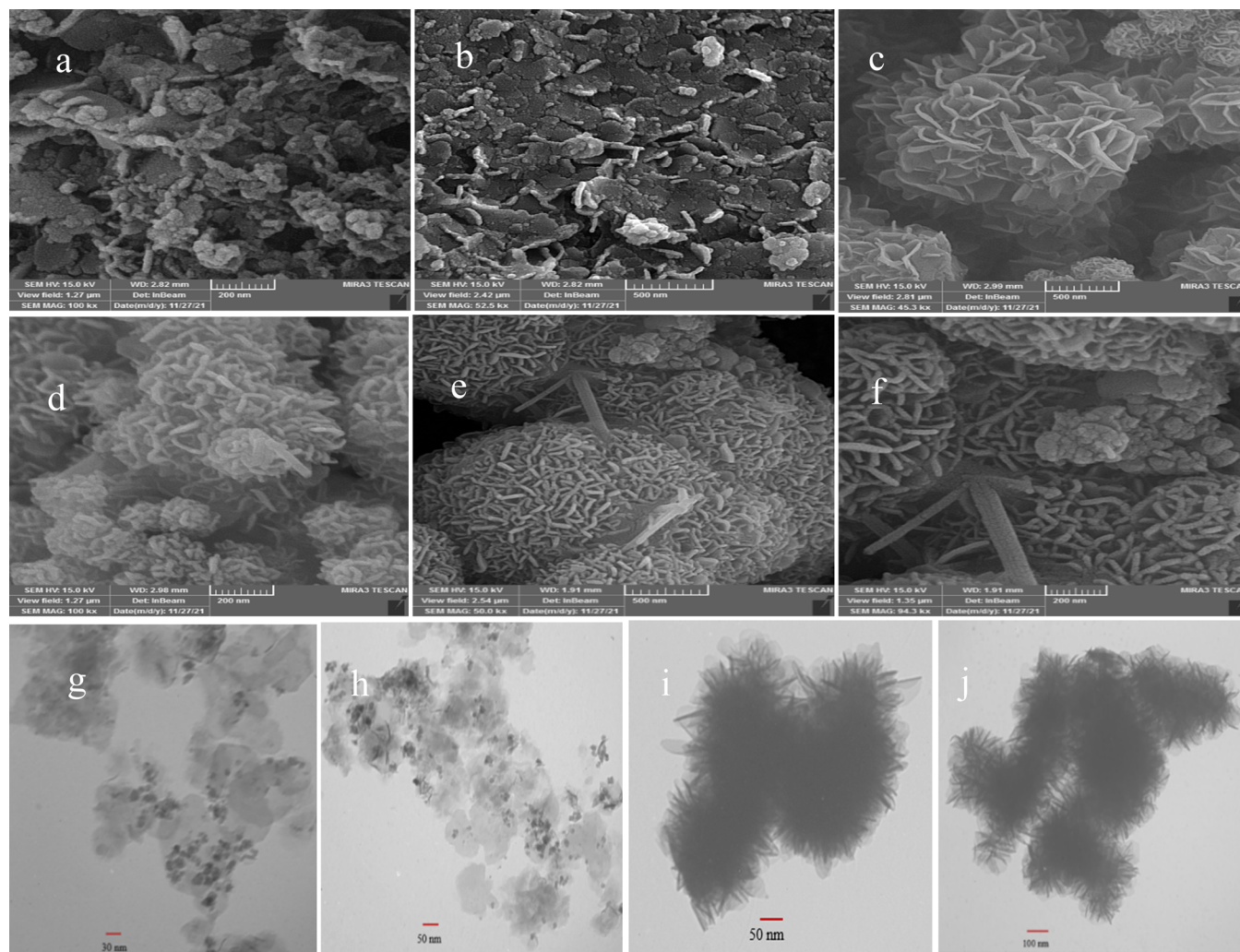
Figure 2. SEM images of (a, b) FeCo LDH/NF, (c, d) α-MnO$_2$/NF, and (e, f) α-MnO$_2$/FeCo LDH/NF and TEM images of (g, h) FeCo LDH and (i, j) α-MnO$_2$ nanoparticles.
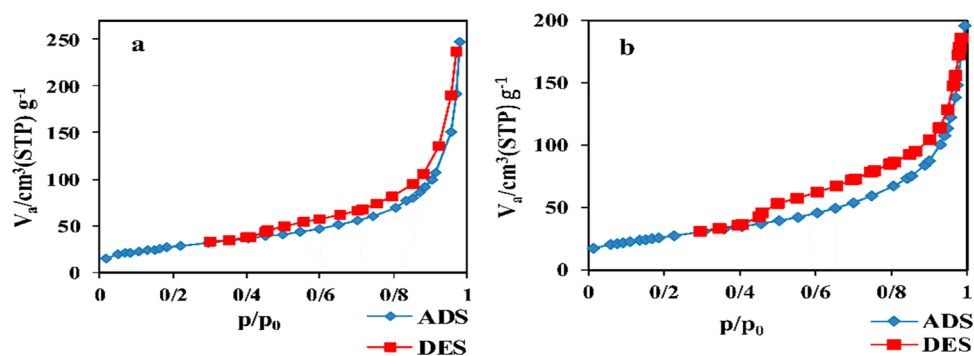

Figure 3. N$_2$ adsorption/desorption isotherms of (a) FeCo LDH and (b) α-MnO$_2$.

stainless steel as the counter electrode. Under these conditions, the scan rate of the measurements was 50 mV S^{-1}. In this study, the potentials vs Ag/AgCl were converted to the reversible hydrogen electrode (RHE) using the Nernst equation:

$$E_{RHE} = E_{Ag/AgCl} + 0.059 \, pH \, (13) + E^0_{Ag/AgCl} \tag{1}$$

$$E^0_{Ag/AgCl} = 0.198 \, V \text{ at } 25^\circ C \tag{2}$$

Electrochemical measurements were performed in the potential range 0−1.8 V vs Ag/AgCl. Linear scanning voltammetry, amperometry, electrochemical impedance spectroscopy (EIS) techniques, and Tafel plots were used to study the electrocatalytic behavior of the synthesized nanostructures. Figure 4a shows the LSV of bare NF, FeCo-LDH/NF, α-MnO$_2$/NF, and α-MnO$_2$/FeCo-LDH/NF. As shown, NF has the lowest electrocatalytic activity, whereas α-MnO$_2$/FeCo-LDH/NF has the best electrocatalytic performance compared to other nanostructures and bare NF. For water oxidation, α-
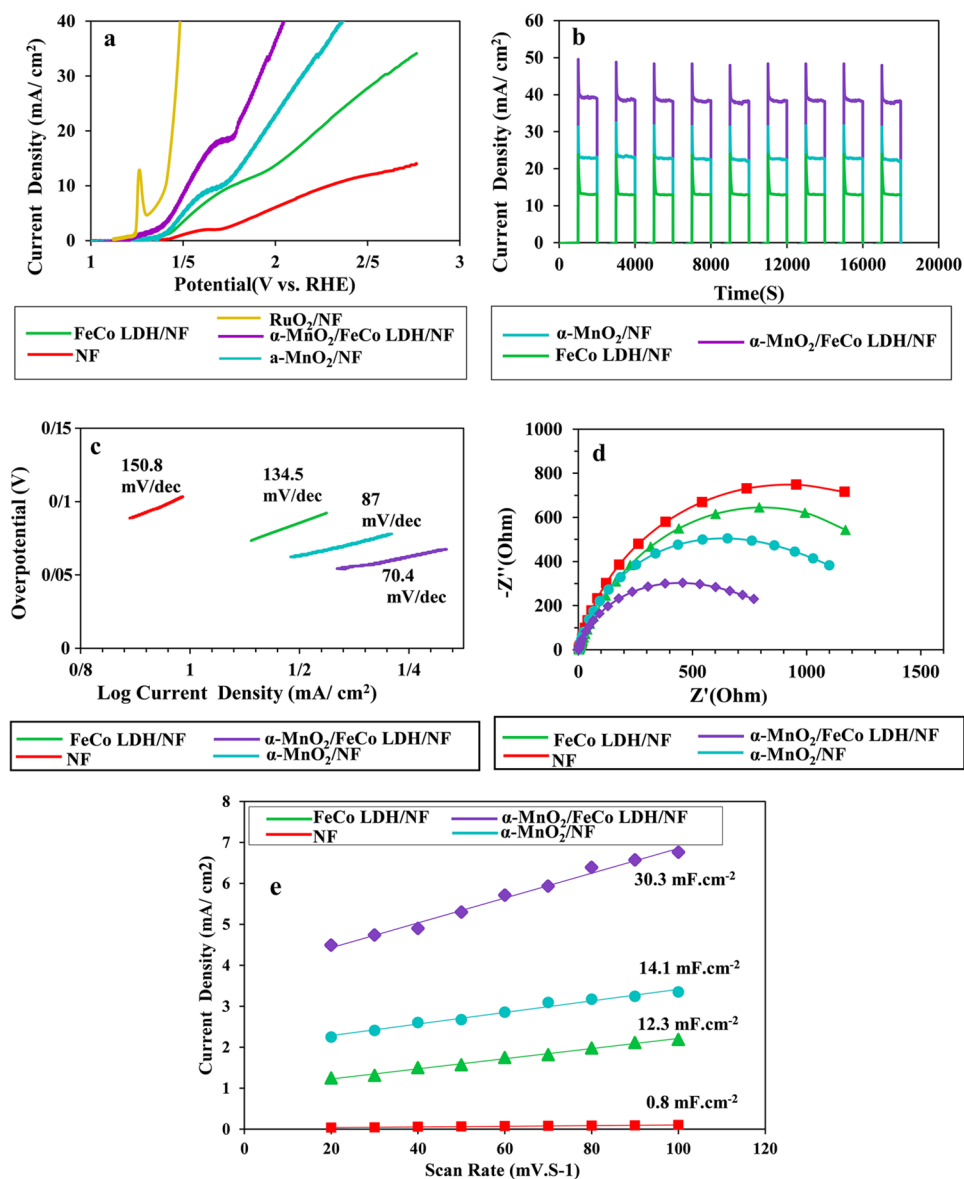
Figure 4. (a) LSV curves, (b) amperometry curves, (c) Tafel plots of synthesized catalysts, (d) Nyquist plots, and (e) double-layer capacitances against scan rates of α-MnO$_2$/FeCo LDH/NF, α-MnO$_2$/NF, FeCo LDH/NF, and NF.

MnO$_2$/FeCo-LDH/NF requires an overpotential of 210 mV to achieve a current density of 5 mA cm^2. The reduction of the oxidation overpotential of water indicates an improvement in the reaction kinetics.

One of the important and practical factors of catalysts is their stability. Amperometric analysis was performed to evaluate the stability of the synthesized products. Figure 4b illustrates the results of this electrochemical test. As can be seen, the repetitive amperometric curves are constant over time, confirming that the synthesized nanostructures have good electrocatalytic performance with high stability. The Tafel curve was plotted to evaluate the electrocatalytic kinetics. Figure 4c shows that the Tafel slope of α-MnO$_2$/FeCo-LDH/NF is 70.4 mV dec^{-1}. The Tafel slopes of α-MnO$_2$/NF, FeCo-LDH/NF, and bare NF are 87, 134.5, and 150.8 mV dec^{-1}, respectively, in a 0.1 M KOH solution. The α-MnO$_2$/FeCo-LDH/NF has the lowest Tafel slope (70.4 mV), and the bare NF has the highest Tafel slope (150.8 mV). The lower slope

indicates an improvement in the catalytic properties and faster kinetics of the water oxidation reaction.

Electrochemical impedance spectroscopy was performed to study the kinetics and electrical conductivity of the water oxidation reaction. Figure 4d shows Nyquist plots for bare NF, FeCo-LDH/NF, α-MnO$_2$/NF, and α-MnO$_2$/FeCo-LDH/NF electrodes. The circuit potential of the electrochemical measurement was in a frequency range of 0.01 Hz to 100 kHz, and the electrolyte was a 0.1 M KOH solution. When the diameter of the semicircle in the diagram is small, the charge transfer resistance (Rct) decreases, which means that the electron transfer kinetics is faster. As shown in the Nyquist diagrams, α-MnO$_2$/FeCo-LDH/NF has the lowest Rct and the highest electrical conductivity compared to other electrodes. Therefore, the electrocatalytic performance of the electrode modified with α-MnO$_2$ and FeCo-LDH is improved.

To better understand the effect of the catalyst's activity on the OER process performance, the effect of the electrochemical

Table 1. Electrocatalytic OER Performance of the Different Catalysts

catalyst	electrolyte	substrate	η_J (mV)	Tafel slop (mV dec^{-1})	reference
$ZnFe_2O_4@ZnFe_2S_4$	1.0 M KOH	NF	η_5-222	73	30
Ni-S-P	1.0 M KOH	NF	η_{10}-219	82	31
Ni-Fe-P	1.0 M KOH	NF	η_{10}-251	75	32
CuP_{300}	1.0 M KOH	NF	η_{10}-310	88	33
CoMoV-LDH	1.0 M KOH	NF	η_{10}-270	106	34
$Ni_3V_1Fe_1$ LDH	1.0 M KOH	glassy carbon electrodes	η_{10}-269	67	35
$Pt-CoS_2$	1.0 M KOH	carbon cloth	η_{10}-300	58	36
$NiS_{0.5}Se_{0.5}$	1.0 M KOH	NF	η_{10}-257	61	37
$Fe_{0.4}Co_{0.6}Se_2$	1.0 M KOH	Co—Fe precursors	η_{10}-270	36	38
$W-NiS_{0.5}Se_{0.5}$	1.0 M KOH	NF	η_{10}-171	41	39
α-MnO_2/FeCo LDH	0.1 M KOH	NF	η_5-210	70.4	this work

surface areas (ECSAs) was estimated using double-layer capacitance (C_{dl}). To accomplish this, the cyclic voltammograms (CVs) were measured in a non-Faradaic region of 1.10 to 1.20 V vs RHE at scan rates of 20−100 mV S^{-1} in 0.1 M KOH. As shown in Figure 4e, the corresponding C_{dl} value of α-MnO_2/FeCo-LDH/NF is 30.3 mF cm^{-2}, which is higher than those of α-MnO_2/NF (14.1 mF cm^{-2}), FeCo-LDH/NF (12.3 mF cm^{-2}), and bare NF (0.8 mF cm^{-2}) electrodes. Furthermore, the ECSA values of the catalysts were estimated via C_{dl} values obtained in Figure 4e and eq 3. The value of specific capacitance (C_s) is 0.040 mF cm^{-2}.[29] ECSA values of 20.0, 307.5, 352.5 and 757.5 m^2 g^{-1} were estimated for bare NF, FeCo-LDH/NF, α-MnO_2/NF and α-MnO_2/FeCo-LDH/NF, respectively.

These results show that the α-MnO_2/FeCo-LDH/NF electrode possesses the largest ECSA, which indicates more active sites in the OER process. Thus, the higher activity of α-MnO_2/FeCo-LDH/NF may be due to the large active surface area and improved rate of charge transfer.

$$ECSA = C_{dl}/C_s \tag{3}$$

Table 1 compares the results of this study with data from previous works and shows that the kinetics of the water oxidation reaction was improved in this work.

4. CONCLUSIONS

In summary, a low-cost and simple hydrothermal method was applied to the synthesis of α-MnO_2/FeCo-LDH nanoparticles on nickel foam, which can also be used to produce nanoparticles on a large scale. α-MnO_2/FeCo-LDH/NF exhibits high electrocatalytic properties in the oxygen evolution reaction, which is due to the improvement of electron transfer rate due to its porous structure and active electrocatalytic sites. For this electrocatalyst, the initial potential for the water oxidation reaction is 0.23 mV vs Ag/AgCl. To achieve a current density of 5 mA cm^2, an overpotential of 210 mV is required, which improves the performance in water oxidation compared to existing reports. The Tafel slope of the modified electrode with α-MnO_2/FeCo-LDH was 70.4 mV dec^{-1} in an alkaline solution. This low Tafel slope indicates the high electrocatalytic performance of the electrode in the water oxidation reaction. The results of our research show that the electrocatalyst has a highly active area, which led to a decrease in charge transfer resistance and improved catalytic activity. This study presents a new approach for the preparation of efficient catalysts for water oxidation reactions based on transition metals.

ASSOCIATED CONTENT

Supporting Information

The Supporting Information is available free of charge at https://pubs.acs.org/doi/10.1021/acsomega.2c07580.

EDS spectra, SEM, and the corresponding elemental mapping images of FeCo LDH, α-MnO_2, and α-MnO_2/FeCo LDH (PDF)

AUTHOR INFORMATION

Corresponding Author

Karim Asadpour-Zeynali − Department of Analytical Chemistry, Faculty of Chemistry, University of Tabriz, Tabriz 5166616471, Iran; Pharmaceutical Analysis Research Center, Faculty of Pharmacy, Tabriz University of Medical Sciences, Tabriz 51664, Iran; orcid.org/0000-0001-9820-552X; Email: asadpour@tabrizu.ac.ir

Author

Saeedeh Shahparast − Department of Analytical Chemistry, Faculty of Chemistry, University of Tabriz, Tabriz 5166616471, Iran

Complete contact information is available at:
https://pubs.acs.org/10.1021/acsomega.2c07580

Notes

The authors declare no competing financial interest.

REFERENCES

(1) (a) Chen, Y.; Yu, J.; Jia, J.; Liu, F.; Zhang, Y.; Xiong, G.; Zhang, R.; Yang, R.; Sun, D.; Liu, H.; Zhou, W. Metallic Ni_3Mo_3N porous microrods with abundant catalytic sites as efficient electrocatalyst for large current density and superstability of hydrogen evolution reaction and water splitting. *Appl. Catal., B* **2020**, *272*, No. 118956. (b) Ismael, M. A review and recent advances in solar-to-hydrogen energy conversion based on photocatalytic water splitting over doped-TiO_2 nanoparticles. *Solar Energy* **2020**, *211*, 522−546. (c) Wang, T.; Zhang, X.; Zhu, X.; Liu, Q.; Lu, S.; Asiri, A. M.; Luo, Y.; Sun, X. Hierarchical CuO@ ZnCo LDH heterostructured nanowire arrays toward enhanced water oxidation electrocatalysis. *Nanoscale* **2020**, *12*, 5359−5362. (d) Tong, M.; Wang, L.; Yu, P.; Liu, X.; Fu, H. 3D Network nanostructured NiCoP nanosheets supported on N-doped carbon coated Ni foam as a highly active bifunctional electrocatalyst for hydrogen and oxygen evolution reactions. *Front. Chem. Sci. Eng.* **2018**, *12*, 417−424.

(2) (a) Manoharan, Y.; Hosseini, S. E.; Butler, B.; Alzhahrani, H.; Senior, B. T. F.; Ashuri, T.; Krohn, J. Hydrogen fuel cell vehicles; current status and future prospect. *Appl. Sci.* **2019**, *9*, 2296. (b) Selvam, N. C. S.; Du, L.; Xia, B. Y.; Yoo, P. J.; You, B. Reconstructed water oxidation electrocatalysts: the impact of surface dynamics on intrinsic activities. *Adv. Funct. Mater.* **2021**, *31*, 2008190. (c) Shamsi, H.*Economic, Environmental, and Health Impact Analysis of Developing Hydrogen Economy in Canada*. 2022

(3) Duan, H.; Li, D.; Tang, Y.; He, Y.; Ji, S.; Wang, R.; Lv, H.; Lopes, P. P.; Paulikas, A. P.; Li, H.; Mao, S. X.; Wang, C.; Markovic, N. M.; Li, J.; Stamenkovic, V. R.; Li, Y. High-performance Rh_2P electrocatalyst for efficient water splitting. *J. Am. Chem. Soc.* **2017**, *139*, 5494−5502.

(4) (a) Mohammadpour, E.; Asadpour-Zeynali, K. α-Fe_2O_3@MoS_2 nanostructure as an efficient electrochemical catalyst for water oxidation. *Microchem. J.* **2020**, *157*, No. 104939. (b) Mohammadpour, E.; Asadpour-Zeynali, K. Ni_3S_2 nanosheets decorated on $NiCo_2O_4$ flakes-arrays directional growth of Ni foam for enhanced electrochemical hydrogen generation. *J. Electroanal. Chem.* **2022**, *908*, No. 116110.

(5) (a) Jiang, N.; Zhu, Z.; Xue, W.; Xia, B. Y.; You, B. Emerging Electrocatalysts for Water Oxidation under Near-Neutral CO_2 Reduction Conditions. *Adv. Mater.* **2022**, *34*, 2105852. (b) Nejati, K.; Davari, S.; Akbari, A.; Asadpour-Zeynali, K.; Rezvani, Z. A highly active oxygen evolution electrocatalyst: Ni-Fe-layered double hydroxide intercalated with the Molybdate and Vanadate anions. *Int. J. Hydrogen Energy* **2019**, *44*, 14842−14852.

(6) (a) Rodrigues, M. P. D. S.; Miguel, V. M.; Germano, L. D.; Córdoba De Torresi, S. I. Metal oxides as electrocatalysts for water splitting: On plasmon-driven enhanced activity. *Electrochem. Sci. Adv.* **2022**, *2*, No. e2100079. (b) Rong, F.; Zhao, J.; Su, P.; Yao, Y.; Li, M.; Yang, Q.; Li, C. Zinc−cobalt oxides as efficient water oxidation catalysts: the promotion effect of ZnO. *J. Mater. Chem. A* **2015**, *3*, 4010−4017. (c) Wang, Z.; Long, X.; Yang, S. Effects of metal combinations on the electrocatalytic properties of transition-metal-based layered double hydroxides for water oxidation: a perspective with insights. *ACS Omega* **2018**, *3*, 16529−16541. (d) Yang, L.; Liu, Z.; Zhu, S.; Feng, L.; Xing, W. Ni-based layered double hydroxide catalysts for oxygen evolution reaction. *Mater. Today Phys.* **2021**, *16*, No. 100292. (e) Zhang, L.; Fan, Q.; Li, K.; Zhang, S.; Ma, X. First-row transition metal oxide oxygen evolution electrocatalysts: regulation strategies and mechanistic understandings. *Sustainable Energy Fuels* **2020**, *4*, 5417−5432.

(7) (a) Dib, M.; Moutcine, A.; Ouchetto, H.; Chtaini, A.; Hafid, A.; Khouili, M. New efficient modified carbon paste electrode by Fe_2O_3@Ni/Al-LDH magnetic nanocomposite for the electrochemical detection of mercury. *Inorg. Chem. Commun.* **2021**, *131*, No. 108624. (b) Sohrabi, H.; Khataee, A.; Ghasemzadeh, S.; Majidi, M. R.; Orooji, Y. Layer double hydroxides (LDHs)-based electrochemical and optical sensing assessments for quantification and identification of heavy metals in water and environment samples: a review of status and prospects. *Trends Environ. Anal. Chem.* **2021**, *31*, No. e00139.

(8) Morimoto, K.; Tamura, K.; Anraku, S.; Sato, T.; Suzuki, M.; Yamada, H. Synthesis of Zn−Fe layered double hydroxides via an oxidation process and structural analysis of products. *J. Solid State Chem.* **2015**, *228*, 221−225.

(9) Kubo, D.; Tadanaga, K.; Hayashi, A.; Tatsumisago, M. Fabrication of Mg-Al Layered Double Hydroxide Thin Membrane for All-Solid-State Alkaline Fuel Cell Using Glass Paper as a Support. *Front. Mater.* **2020**, *7*, 117.

(10) Wang, Y.; Tao, S.; Lin, H.; Wang, G.; Zhao, K.; Cai, R.; Tao, K.; Zhang, C.; Sun, M.; Hu, J.; Huang, B.; Yang, S. Atomically targeting NiFe LDH to create multivacancies for OER catalysis with a small organic anchor. *Nano Energy* **2021**, *81*, No. 105606.

(11) Sohrabnezhad, S.; Poursafar, Z.; Asadollahi, A. Synthesis of novel of MgAl layered double hydroxide@ porous magnetic shell () as carrier for ciprofloxacin drug. *Appl. Clay Sci.* **2020**, *190*, No. 105586.

(12) Yang, W.; Li, J.; Wang, M.; Sun, X.; Liu, Y.; Yang, J.; Ng, D. H. A colorimetric strategy for ascorbic acid sensing based on the peroxidase-like activity of core-shell Fe3O4/CoFe-LDH hybrid. *Colloids Surf., B* **2020**, *188*, No. 110742.

(13) Soltani, R.; Marjani, A.; Shirazian, S. A hierarchical LDH/MOF nanocomposite: single, simultaneous and consecutive adsorption of a reactive dye and Cr (vi). *Dalton Trans.* **2020**, *49*, 5323−5335.

(14) Wu, K.; Xu, S.; Tian, X.-Y.; Zeng, H.-Y.; Hu, J.; Guo, Y.-H.; Jian, J. Renewable lignin-based surfactant modified layered double hydroxide and its application in polypropylene as flame retardant and smoke suppression. *Int. J. Biol. Macromol.* **2021**, *178*, 580−590.

(15) Wang, Y.; Yan, D.; El Hankari, S.; Zou, Y.; Wang, S. Recent progress on layered double hydroxides and their derivatives for electrocatalytic water splitting. *Adv. Sci.* **2018**, *5*, 1800064.

(16) (a) He, W.; Han, L.; Hao, Q.; Zheng, X.; Li, Y.; Zhang, J.; Liu, C.; Liu, H.; Xin, H. L. Fluorine-anion-modulated electron structure of nickel sulfide nanosheet arrays for alkaline hydrogen evolution. *ACS Energy Lett.* **2019**, *4*, 2905−2912. (b) Qian, J.; Wang, T.; Xia, B.; Xi, P.; Gao, D. Zn-doped $MoSe_2$ nanosheets as high-performance electrocatalysts for hydrogen evolution reaction in acid media. *Electrochim. Acta* **2019**, *296*, 701−708. (c) Yang, J.; Yu, C.; Hu, C.; Wang, M.; Li, S.; Huang, H.; Bustillo, K.; Han, X.; Zhao, C.; Guo, W.; Zeng, Z.; Zheng, H.; Qiu, J. Surface-confined fabrication of ultrathin nickel cobalt-layered double hydroxide nanosheets for high-performance supercapacitors. *Adv. Funct. Mater.* **2018**, *28*, 1803272. (d) Zheng, Y.; Jiao, Y.; Vasileff, A.; Qiao, S. Z. The hydrogen evolution reaction in alkaline solution: from theory, single crystal models, to practical electrocatalysts. *Angew. Chem., Int. Ed.* **2018**, *57*, 7568−7579.

(17) Zhang, B.; Li, Y.; Valvo, M.; Fan, L.; Daniel, Q.; Zhang, P.; Wang, L.; Sun, L. Electrocatalytic Water Oxidation Promoted by 3 D Nanoarchitectured Turbostratic δ-MnO_x on Carbon Nanotubes. *ChemSusChem* **2017**, *10*, 4472−4478.

(18) Teng, Y.; Wang, X. D.; Liao, J. F.; Li, W. G.; Chen, H. Y.; Dong, Y. J.; Kuang, D. B. Atomically thin defect-rich Fe−Mn−O hybrid nanosheets as high efficient electrocatalyst for water oxidation. *Adv. Funct. Mater.* **2018**, *28*, 1802463.

(19) (a) Balaghi, S. E.; Triana, C. A.; Patzke, G. R. Molybdenum-doped manganese oxide as a highly efficient and economical water oxidation catalyst. *ACS Catal.* **2020**, *10*, 2074−2087. (b) Maayan, G.; Gluz, N.; Christou, G. A bioinspired soluble manganese cluster as a water oxidation electrocatalyst with low overpotential. *Nat. Catal.* **2018**, *1*, 48−54. (c) Simchi, H.; Cooley, K. A.; Ohms, J.; Huang, L.; Kurz, P.; Mohney, S. E. Cosputtered calcium manganese oxide electrodes for water oxidation. *Inorg. Chem.* **2018**, *57*, 785−792.

(20) Cheng, F.; Zhao, J.; Song, W.; Li, C.; Ma, H.; Chen, J.; Shen, P. Facile controlled synthesis of MnO_2 nanostructures of novel shapes and their application in batteries. *Inorg. Chem.* **2006**, *45*, 2038−2044.

(21) Wu, H.; Zhao, Z.; Wu, G. Facile synthesis of FeCo layered double oxide/raspberry-like carbon microspheres with hierarchical structure for electromagnetic wave absorption. *J. Colloid Interface Sci.* **2020**, *566*, 21−32.

(22) Foruzin, L. J.; Rezvani, Z.; Shishavan, Y. H.; Habibi, B. $Ni_2Zn_{0.5}Fe$-LDH modified carbon paste electrode as an efficient electrocatalyst for water oxidation in neutral media. *Int. J. Hydrogen Energy* **2018**, *43*, 150−160.

(23) Yuan, Y.; Tong, C.; Lü, C. Mussel-inspired functionalized LDH as covalent crosslinkers for constructing micro-crosslinking fluorenyl-containing polysulfone-based composite anion exchange membranes with enhanced properties. *Appl. Clay Sci.* **2020**, *199*, No. 105878.

(24) Zhuk, N. A.; Ipatova, E. U.; Makeev, B. A.; Nekipelov, S. V.; Beznosikov, D. S.; Rychkova, L. V.*NEXAFS and FTIR Spectroscopy of Co-doped SrBi2Nb2O9*. 2022.

(25) (a) Khan, M. A.; Islam, M.; Ishaque, M.; Rahman, I.; Genson, A.; Hampshire, S. Structural and physical properties of Ni−Tb−Fe−O system. *Mater. Charact.* **2009**, *60*, 73−78. (b) Song, H.; Zhang, X.; Chen, T.; Jia, X. One-pot synthesis of bundle-like β-FeOOH nanorods and their transformation to porous α-Fe_2O_3 microspheres. *Ceram. Int.* **2014**, *40*, 15595−15602.

(26) Sivakumar, S.; Prabu, L. N. Synthesis and Characterization of α-MnO$_2$ nanoparticles for Supercapacitor application. *Mater. Today: Proc.* **2021**, *47*, 52−55.

(27) (a) Kuang, X.; Kang, B.; Wang, Z.; Gao, L.; Guo, C.; Lee, J. Y.; Sun, X.; Wei, Q. Sulfur-Doped CoO Nanoflakes with Loosely Packed Structure Realizing Enhanced Oxygen Evolution Reaction. *Chem. — Eur. J.* **2018**, *24*, 17288−17292. (b) Singha, A.; Das, P. K.; Dey, A. Resonance Raman spectroscopy and density functional theory calculations on ferrous porphyrin dioxygen adducts with different axial ligands: correlation of ground state wave function and geometric parameters with experimental vibrational frequencies. *Inorg. Chem.* **2019**, *58*, 10704−10715.

(28) Radinger, H.; Connor, P.; Stark, R.; Jaegermann, W.; Kaiser, B. Manganese Oxide as an Inorganic Catalyst for the Oxygen Evolution Reaction Studied by X-Ray Photoelectron and Operando Raman Spectroscopy. *ChemCatChem* **2021**, *13*, 1175−1185.

(29) McCrory, C. C.; Jung, S.; Peters, J. C.; Jaramillo, T. F. Benchmarking heterogeneous electrocatalysts for the oxygen evolution reaction. *J. Am. Chem. Soc.* **2013**, *135*, 16977−16987.

(30) Mohammadpour, E.; Asadpour-Zeynali, K. ZnFe$_2$O$_4$@ ZnFe$_2$S$_4$ core-shell nanosheet on Ni foam as efficient and novel electrocatalyst for oxygen generation. *Int. J. Hydrogen Energy* **2021**, *46*, 26940−26949.

(31) Xu, Q.; Gao, W.; Wang, M.; Yuan, G.; Ren, X.; Zhao, R.; Zhao, S.; Wang, Q. Electrodeposition of NiS/Ni$_2$P nanoparticles embedded in amorphous Ni (OH)$_2$ nanosheets as an efficient and durable dual-functional electrocatalyst for overall water splitting. *Int. J. Hydrogen Energy* **2020**, *45*, 2546−2556.

(32) Xuan, C.; Peng, Z.; Xia, K.; Wang, J.; Xiao, W.; Lei, W.; Gong, M.; Huang, T.; Wang, D. Self-supported ternary Ni-Fe-P nanosheets derived from metal-organic frameworks as efficient overall water splitting electrocatalysts. *Electrochim. Acta* **2017**, *258*, 423−432.

(33) Pawar, S. M.; Pawar, B. S.; Babar, P. T.; Ahmed, A. T. A.; Chavan, H. S.; Jo, Y.; Cho, S.; Kim, J.; Inamdar, A. I.; Kim, J. H. Electrosynthesis of copper phosphide thin films for efficient water oxidation. *Mater. Lett.* **2019**, *241*, 243−247.

(34) Bao, J.; Wang, Z.; Xie, J.; Xu, L.; Lei, F.; Guan, M.; Zhao, Y.; Huang, Y.; Li, H. A ternary cobalt−molybdenum−vanadium layered double hydroxide nanosheet array as an efficient bifunctional electrocatalyst for overall water splitting. *Chem. Commun.* **2019**, *55*, 3521−3524.

(35) Wang, Z.; Liu, W.; Hu, Y.; Xu, L.; Guan, M.; Qiu, J.; Huang, Y.; Bao, J.; Li, H. An Fe-doped NiV LDH ultrathin nanosheet as a highly efficient electrocatalyst for efficient water oxidation. *Inorg. Chem. Front.* **2019**, *6*, 1890−1896.

(36) Han, X.; Wu, X.; Deng, Y.; Liu, J.; Lu, J.; Zhong, C.; Hu, W. Ultrafine Pt nanoparticle-decorated pyrite-type CoS$_2$ nanosheet arrays coated on carbon cloth as a bifunctional electrode for overall water splitting. *Adv. Energy Mater.* **2018**, *8*, 1800935.

(37) Wang, Y.; Li, X.; Zhang, M.; Zhou, Y.; Rao, D.; Zhong, C.; Zhang, J.; Han, X.; Hu, W.; Zhang, Y.; Zaghib, K.; Wang, Y.; Deng, Y. Lattice-Strain Engineering of Homogeneous NiS$_{0.5}$Se$_{0.5}$ Core−Shell Nanostructure as a Highly Efficient and Robust Electrocatalyst for Overall Water Splitting. *Adv. Mater.* **2020**, *32*, 2000231.

(38) Wang, C.; Yan, B.; Chen, Z.; You, B.; Liao, T.; Zhang, Q.; Lu, Y.; Jiang, S.; He, S. Recent Advances on Carbon Substrates Supported Nonprecious Nanoarrays for Electrocatalytic Oxygen Evolution. *J. Mater. Chem. A* **2021**, 25773.

(39) Wang, Y.; Li, X.; Zhang, M.; Zhang, J.; Chen, Z.; Zheng, X.; Tian, Z.; Zhao, N.; Han, X.; Zaghib, K.; Wang, Y.; Deng, Y.; Hu, W. Highly Active and Durable Single-Atom Tungsten-Doped NiS$_{0.5}$Se$_{0.5}$ Nanosheet@ NiS$_{0.5}$Se$_{0.5}$ Nanorod Heterostructures for Water Splitting. *Adv. Mater.* **2022**, *34*, 2107053.